REVIEWS

Journal of Semiconductors
(2019) 40, 081505
doi: 10.1088/1674-4926/40/8/081505

Advances in new generation diluted magnetic semiconductors with independent spin and charge doping

Guoqiang Zhao[1, 2], Zheng Deng[1, 2], and Changqing Jin[1, 2, †]

[1]Institute of Physics, Chinese Academy of Sciences, Beijing 100190, China
[2]School of Physics, University of Chinese Academy of Sciences, Beijing, 100190, China

Abstract: As one branch of spintronics, diluted magnetic semiconductors (DMSs) are extensively investigated due to their fundamental significance and potential application in modern information society. The classical materials (Ga,Mn)As of III–V group based DMSs has been well studied for its high compatibility with the high-mobility semiconductor GaAs. But the Curie temperature in (Ga,Mn)As film is still far below room temperature because the spin & charge doping is bundled to the same element that makes the fabrication very difficult. Alternatively, the discovery of a new generation DMSs with independent spin and charge doping, such as (Ba,K)$(Zn,Mn)_2As_2$ (briefly named BZA), attracted considerable attention due to their unique advantages in physical properties and heterojunction fabrication. In this review we focus on this series of new DMSs including (I) materials in terms of three types of new DMSs, i.e. the "111", "122" and "1111" system; (II) the physical properties of BZA; (III) single crystals & prototype device based on BZA. The prospective of new type of DMSs with independent spin and charge doping is briefly discussed.

Key words: diluted magnetic semiconductors; independent spin and charge doping; high Curie temperature

Citation: G Q Zhao, Z Deng, and C Q Jin, Advances in new generation diluted magnetic semiconductors with independent spin and charge doping[J]. *J. Semicond.*, 2019, 40(8), 081505. http://doi.org/10.1088/1674-4926/40/8/081505

1. Introduction

It is an everlasting dream to make electronic devices miniaturization, multi-functionalization, intellectualization, and low-power consumption in this current information society[1]. But many bottleneck problems occur when the fabrication technology encounter nanometer scale[2]. As one branch of spintronics, diluted magnetic semiconductors (DMSs) offers intriguing opportunities to combine semiconductor properties and ferromagnetism in a single material that would enable to fabricate new devices to process and store information simultaneously[3, 4].

DMSs researches date back to the concentrated magnetic semiconductors compounds, like EuX[5] (X = O, S, Se and Te) & $CdCr_2X_4$[6] (X = S and Se). However, the complicated growth and the relatively low Curie temperature (T_C) for these compounds limited these materials to fundamental studies. In 1980s, people payed much attention to Mn doped II–VI group DMSs, such as (Zn,Mn)Te, (Zn,Mn)Se, (Cd,Mn)Te, etc[7] and PbSnMnTe[8]. Yet T_C is still only several Kelvins due to lack of effective approach to dope carriers[9]. Benefiting from the low temperature molecular beam epitaxy (LT-MBE) technique, Mn doped III–V group DMSs were explored in 1990s, like (Ga,Mn)As[10–12] and (In,Mn)As[13]. The highest T_C could reach 200 K in heavy Mn doped (Ga,Mn)As film with proper annealing procedure[14–16].

It is of great fundamental significance and practical value to further improve T_C of (Ga,Mn)As[17, 18]. However, in (Ga,Mn)As, the Ga^{3+}/Mn^{2+} substitution offers hole carriers and spins simultaneously, which make it difficult to individually control charge and spin concentrations and more importantly to improve T_C. Since 2011, a new type of DMSs with independent spin and charge doping, such as the "111" type Li(Zn,Mn)As[19] and "122" type (Ba,K)$(Zn,Mn)_2As_2$ (BZA)[20] named by its stoichiometry ratio, have been discovered. In these DMSs[21], such as BZA, spins are introduced by isovalent Zn^{2+}/Mn^{2+} doping, and charge carriers are introduced by heterovalent Ba^{2+}/K^{1+} substitution. Taking the advantage of freedom to individually control of charge and spin, BZA exhibit ferromagnetic order with T_C up to 230 K[22] which is record of controlled reliable T_C among carrier mediated ferromagnetic DMSs[16]. In this review, we demonstrate the discovery of three basic groups of new DMSs, namely the "111", "122" and "1111" families (Fig. 1). Then we focus on physical properties of BZA and prototype device based on BZA single crystal. In the last section, we discuss the prospective of new type of DMSs with independent spin and charge doping.

2. Polycrystals synthesis and basic physicial properties

2.1. "111" type DMSs

LiZnAs[23, 24] is a direct-gap semiconductor that has a cubic crystal structure with space group F-43m as shown in Figs. 1(a) & 1(b) and a band gap (1.61 eV) similar to that of GaAs[25] (1.52 eV). Note that LiZnAs could be viewed as a zinc blende structure, in which Ga sites in (Ga,As) are replaced with Li and Zn. Benefitting on the LiFeAs[26] iron superconductor fabrication experiences and facilities. Jin's group firstly reported the successful synthesis of bulk form polycrystals Li(Zn,Mn)As[19]. In principle, the Zn^{2+}/Mn^{2+} replacement offers spins, and the off-stoichiometrical Li cation adjust the carrier's type and concentration. But the long range ferromagnetic ordering was only observed with the excess Li doping and it is a

Correspondence to: C Q Jin, Jin@iphy.ac.cn
Received 18 JULY 2019; Revised 2 AUGUST 2019.

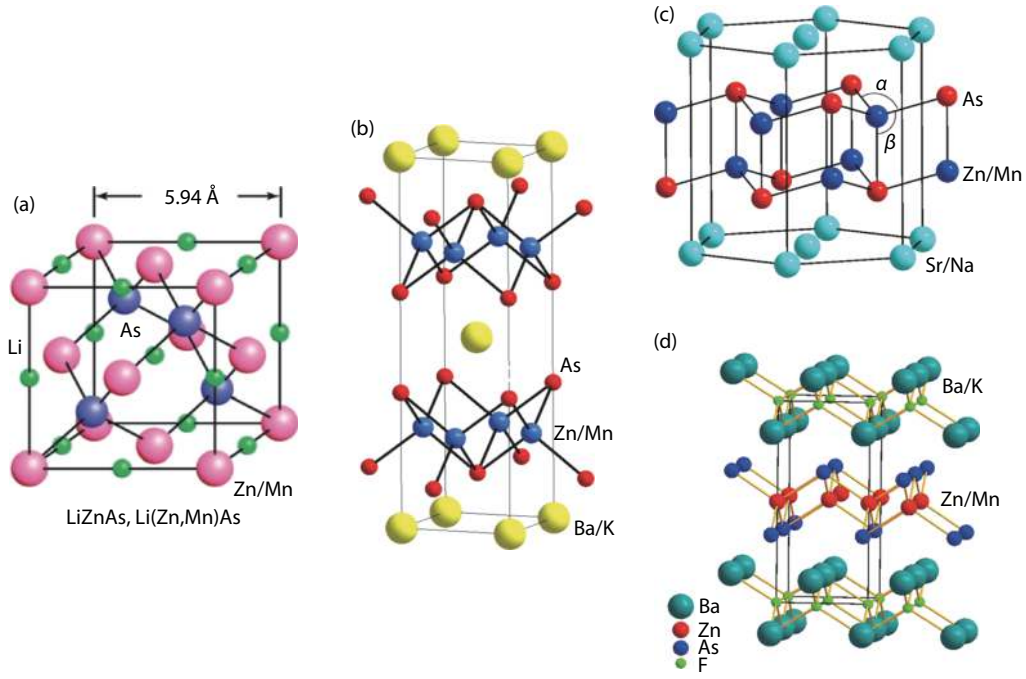

Fig. 1. (Color online) The crystal structure of (a) "111" Li(Zn,Mn)As with zinc blende structure, (b) "122" (Ba,K)$(Zn,Mn)_2As_2$ with $ThCr_2Si_2$ type structure, (c) (Sr,Na)$(Zn,Mn)_2As_2$ with $CaAl_2Si_2$ type structure, (d) "1111" (Ba,K)F(Zn,Mn)As with ZrCuSiAs structure. Adoped from Refs. [19, 20, 42, 47].

p-type rather than n-type as the theory prediction[27]. The reason is that the excess Li^{1+} prefers to occupy the Zn^{2+} sites based on a DFT calculation[28]. The temperature dependence of M at 2 kOe (no difference between field cooling and zero field cooling procedures) was illustrated in Fig. 2(a), and external field H from 0 to 20 kOe dependence of M at 2 K is shown in Fig. 2(b). Clear signatures of ferromagnetic order were seen in these figures with the highest T_C of 50 K in $Li_{1.1}(Zn_{0.85}Mn_{0.15})$ As sample. Semiconducting behavior of resistivity of LiZnAs (green line in Fig. 2(c)) changes to T-independent behavior for Li deficient systems, wheras much smaller resistivity and definite metallic behavior were found for Li excess samples. The resistivity increases monotonically with increasing Mn concentration in Fig. 2(d) which suggests that Mn acts as a scattering center. The onset of magnetic order reduces this scattering rate, as can be seen in the negative magnetoresistance of $Li_{1.1}(Zn_{0.9}Mn_{0.1})As$ sample in Fig. 2(e) below T_C. Fig. 2(f) shows representative anomalous Hall effect of $Li_{1.1}(Zn_{0.95}Mn_{0.05})As$ at 2 K, which exhibits p-type carriers with concentrations of $n \sim 10^{20}$ cm^{-3}.

In order to examine volume fraction and the ordered moment size, μSR measurements were performed on sintered polycrystalline specimens of $Li_{1.1}(Zn_{0.95}Mn_{0.05})As$[29]. The time spectra in zero field (ZF), shown in Fig. 3(a), clearly show an increase of the relaxation rate below ~25 K on Fig. 3(b), and measurements in longitudinal fields confirmed that the increase is from static magnetic order. This is in correspond with the earlier result in (Ga,Mn)As[30]. The volume fraction of regions with static magnetism on Fig. 3(c) indicates a sharp transition at T_C ~ 30 K, and full volume magnetic order achieved when $T < 10$ K. Further studies on fabrication methods and heat treatments might help improve spatial homogeneity of the transition. The weak transverse field (WTF) of 30 Oe, shown in Fig. 3(d), also provide direct signal of the magnetic volume fraction[31]. When the internal magnetic field is much larger than the applied external field, the scale of oscillation can reflect the paramagnetic volume. The consistenct of the ordered fraction from the measurements in ZF and WTF, shown in Fig. 3(c), supports the validity of our analysis of ZF-μSR spectra.

The discovery of Li(Zn,Mn)As sparked extensive researches in this 111 type DMSs[28, 32–36]. Fig. 4 shows only three of these new DMSs with independent spin and charge doping, e.g. Li(Zn,Mn)P, Li(Cd,Mn)P and Li(Zn,Co,Mn)As. Isostructural to Li(Zn,Mn)As[19], Li(Zn,Mn)P[28] is also a p-type DMSs with excess lithium providing charge doping. The highest T_C could reaches 34 K. The saturation moment per Mn (M_{sat}) is about $1\mu_B$–$2\mu_B$, which is comparable to that in (Ga,Mn)As[11], Li(Zn,Mn)As[19], etc. $\rho(T)$ of Li(Zn,Mn)P decreases with increasing temperature, which shows semiconductor behaviors[28]. Li(Zn,Mn)P is a soft magnetic material with about less than 100 Oe, shown in Fig. 4(a), based on the magnetic hysteresis loop and magnetoresistance curves. Magnetoresistivity $\rho_H(T)$ of $Li_{1.04}(Zn_{0.9}Mn_{0.1})P$ at different external fields are shown in Fig. 4(b). $\rho_H(T)$ increases monotonically with decreasing temperature, showing a rapid rise below T_C. As shown in the inset of Fig. 4(b), the negative magnetoresistance is far from saturation in rather high magnetic field, in which spin orientation is fully aligned. In this condition, the negative magnetoresistance presumably results from the weak localization effects[37]. Systematic μSR measurements[32] also confirmed that the magnetic volume fraction on $Li_{1.15}(Zn_{0.9}Mn_{0.1})P$ could reaches nearly 100% at 2 K. Compared to Li(Zn,Mn)P, DMSs Li(Cd,Mn)P[36] with optimum doping exhibits a higher T_C of 45 K as shown in Fig. 4(c). But more than 80% negative magnetoresistance, shown in Fig. 4(d), is a record in this 111 type DMSs. For this new type DMSs, spins and carries are indispensable.

Usually, the carriers are induced in Li site while spins in Zn site in all these above systems. Different from that idea, a new DMSs Li(Zn,Co,Mn)As[33] was reported in which carriers and spins are both induced in Zn site simultaneously. Fig. 4(e) dis-

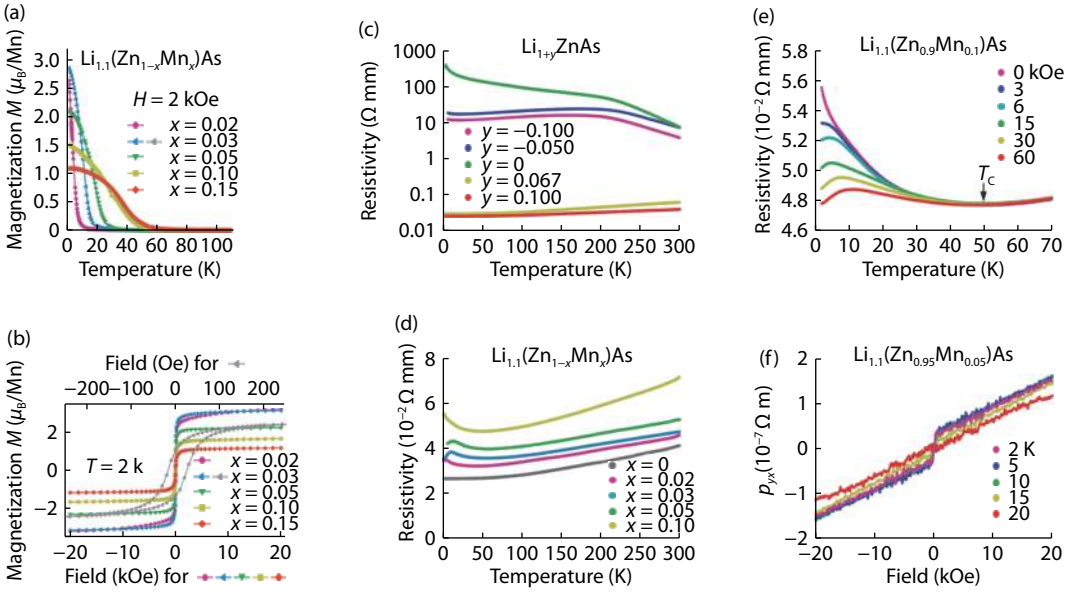

Fig. 2. (Color online) Magnetization & transport measurements of Li(Zn,Mn)As. (a) The temperature dependence of M in $H = 2$ kOe (no difference in FC and ZFC procedures). (b) M at 2 K in various values of external field H from 0 to 20 kOe. The grey symbols show a hysteresis loop in $x = 0.03$ system plotted for smal field regions (top horizontal axis), which demonstrate a very small coercive field of 30–100 Oe. (c) Resistivity of $Li_{1+y}ZnAs$, showing metallic behavior of Li deficient ($y < 0$) and Li excess ($y > 0$) compounds. (d) Resistivity of $Li_{1.1}(Zn_{1-x}Mn_x)As$, showing the effect of increasing charge scattering with increasing Mn concentration x. (e) Resistivity of $Li_{1.1}(Zn_{0.9}Mn_{0.1})As$ in various external field H, which exhibits negative magnetoresistance below $T_C \sim 50$ K. (f) Hall resistivity of $Li_{1.1}(Zn_{0.95}Mn_{0.05})As$ at 2 K, which exhibits p-type carriers with concentrations of $n \sim 10^{20}$ cm^{-3} together with the anomalous Hall effect due to spontaneous magnetization at $H = 0$. Adoped from Ref. [19].

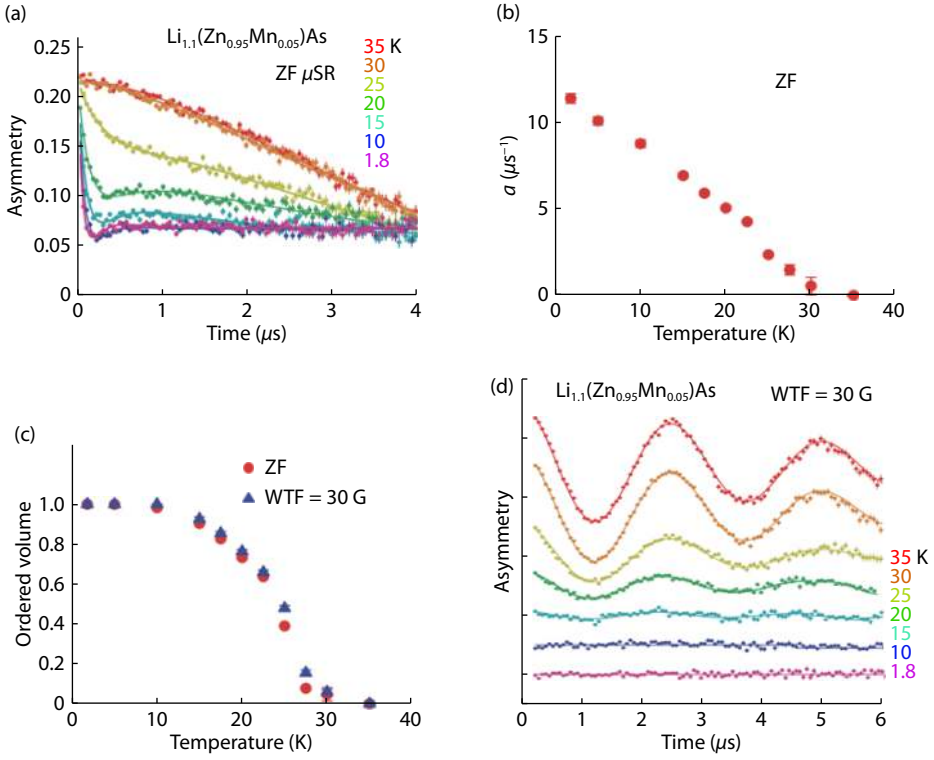

Fig. 3. (Color online) Results of μSR measurements in sintered polycrystalline specimens of $Li_{1.1}(Zn_{0.95}Mn_{0.05})As$. (a) Time spectra in zero field that exhibit onset of extra relaxation below $T \sim 30$ K. The solid lines represent fits to the relaxation function for dilute spin systems in zero field for the static case (often used for dilute alloy spin glasses), which exhibits a fast relaxation, plus a non-relaxing paramagnetic component. (b) The relaxation rate α of the signal that exhibits fast relaxation. (c) The volume fraction of the magnetically ordered region, derived from the amplitude of the fast relaxing signal. (d) μSR time spectra in the WTF of 30 Oe. The oscillation amplitude corresponds to the paramagnetic volume fraction. Adoped from Ref. [19].

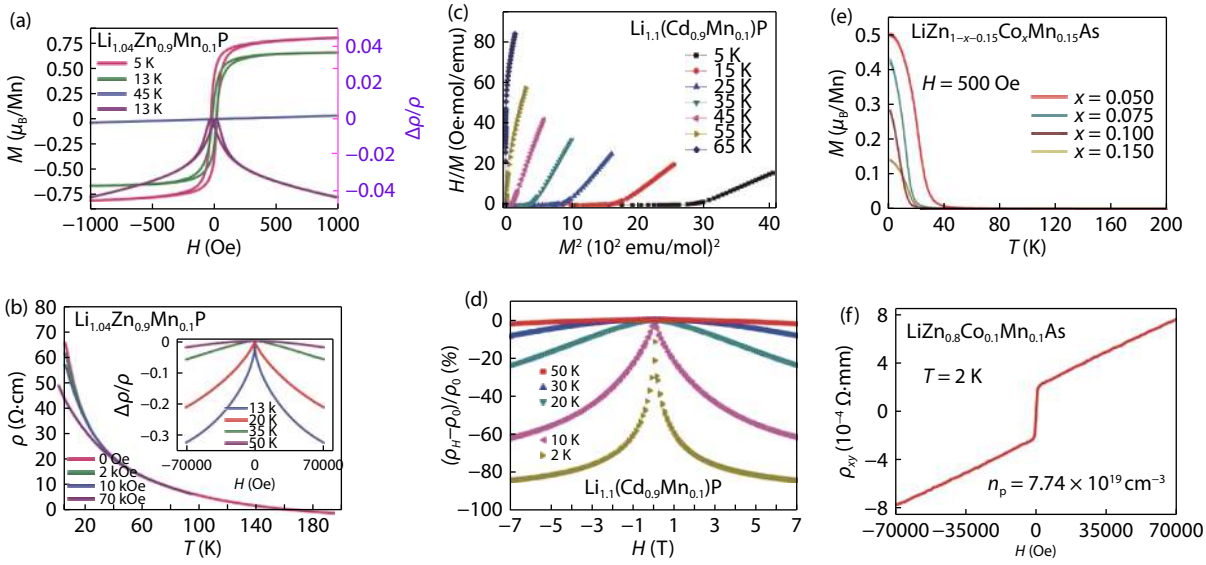

Fig. 4. (Color online) (a) $M(H)$ and $\rho(H)$ in $Li_{1.04}Zn_{0.9}Mn_{0.1}P$ show hysteresis, demonstrating ferromagnetism with small coercive field of about 50 Oe. (b) Magnetoresistivity $\rho_H(T)$ of $Li_{1.04}Zn_{0.9}Mn_{0.1}P$ at different external fields. Inset shows negative magnetoresistance at low temperature. (c) Arrott plots at various temperatures above and below T_C, shows the ferromagnetic transition temperature at 45 K. (d) Negative magnetoresistance at different temperatures. (e) The temperature dependence of M in H = 100 Oe for $Li(Zn_{1-x-0.15}Co_xMn_{0.15})As$ (no difference in ZFC and FC procedures for small coercive fields). (f) Hall resistivity of $Li(Zn_{0.8}Co_{0.1}Mn_{0.1})As$ at 2 K, which exhibits p-type carriers with concentrations of $n \sim 7.74 \times 10^{19}$ cm^{-3} together with the anomalous Hall effect due to spontaneous magnetization at $H = 0$. Adoped from Refs. [28, 33].

plays the tempertature dependence of M in H = 100 Oe for $Li(Zn_{1-x-0.15}Co_xMn_{0.15})P$. There is no difference in ZFC and FC procedures for small coercive fields with the highest T_C of 40 K in $LiZn_{0.80}Co_{0.05}Mn_{0.15}P$. The resistivity of $Li(Zn_{1-x-0.15}Mn_{0.15})P$ decreases with increase of Co doping. This means much more carries are induced successfully. A field induced insulator-to-metal like transition around T_C can be observed with the external field of 1 T, which is due to the suppression of magnetic fluctuations below T_C. This feature is also observed in Li(Zn,Mn)As system[19]. Fig. 4(d) demonstrates the Hall resistivity of $Li(Zn_{0.8}Co_{0.1}Mn_{0.1})As$ at 2 K, which exhibits p-type carriers with concentrations of $n \sim 7.74 \times 10^{19}$ cm^{-3} together with the anomalous Hall effect due to spontaneous magnetization at $H = 0$.

2.2. "122" type DMSs

$BaZn_2As_2$ is a semiconductor synthetized at high temperature (>900 °C) with the tetragonal $ThCr_2Si_2$ crystal structure. A new type "122" DMSs $(Ba,K)(Zn,Mn)_2As_2$ has been synthesized with the Ba^{2+}/K^{1+} substitution (hole carries) and Zn^{2+}/Mn^{2+} (spins) doping. Fig. 5(a) shows the temperature dependence of M in H = 500 Oe for $(Ba_{0.7}K_{0.3})(Zn_{0.85}Mn_{0.15})_2As_2$ at ZFC and FC procedures with T_C 230 K. The hysteresis curves $M(H)$ are shown in the inset of Fig. 5(a). Fig. 5(b) exhibits the spontaneous magnetization curve under 5 Oe of $(Ba_{0.7}K_{0.3})$-$(Zn_{0.85}Mn_{0.15})_2As_2$, showing $T^{3/2}$ dependence in low temperature, as expected for a homogeneous ferromagnet[38]. Volume fraction of regions with static magnetic order, estimated by μSR measurements in ZF and WTF of 50 Oe are shown in Fig. 5(c). The μSR results indicate that static magnetic order develops in the entire volume with a sharp onset around T_C. Resistivity of $(Ba_{1-x}K_x)(Zn_{1-y}Mn_y)_2As_2$ for with several different charge doping levels are shown in Fig. 5(d). For $BaZn_2As_2$ semiconductor, doping K atoms into Ba sites introduces hole carriers, leading to metallic behavior in $(Ba,K)Zn_2As_2$. The resistivity curves of $(Ba_{1-x}K_x)(Zn_{1-y}Mn_y)_2As_2$ for selected values of x up to 0.3, exhibit a small increase at low temperatures due to spin scattering effect caused by Mn dopants. This variation of resistivity is often observed in heavily doped semiconductors[39]. Strictly metallic behavior (with monotonic decrease of resistivity with decreasing temperatures) is not a precondition of having a ferromagnetic coupling between Mn moments mediated by RKKY interaction[12, 30]. Fig. 5(e) shows the magnetoresistance curve measured in the external field up to 7 T at different temperatures, showing obvious negative magnetoresistance below T_C. Fig. 5(f) shows the Hall effect results of $(Ba_{0.85}K_{0.15})(Zn_{0.90}Mn_{0.10})_2As_2$ at several temperatures with hole concentration about 4.3×10^{20} cm^{-3}.

Different from $(Ba,K)(Zn,Mn)_2As_2$, another "122" type DMSs with hexagonal $CaAl_2Si_2$ was reported subsequently, such as $(Ca,Na)(Zn,Mn)_2As_2$[40], $(Sr,Na)(Zn,Mn)_2As_2$[41] and $(Sr,Na)(Cd,Mn)_2As_2$[42], etc. Fig. 6(a) shows the temperature dependence of M in H = 500 Oe for $(Ca_{0.9}Na_{0.1})(Zn,Mn)_2As_2$ with several different charge doping levels at ZFC and FC procedures. The highest T_C is 33 K. In Fig. 6(b), the temperature dependence of the volume fraction of regions with static magnetic order, derived from μSR measurements in ZF, is consistent with that of spontaneous magnetization under 5 Oe. The latter shows $T^{3/2}$ dependence in low temperature expected for a homogeneous ferromagnet[22, 30, 38]. Due to the competition between nearest-neighbor antiferromagnetic interactions and ferromagnetic interactions from remote Mn moments, M_{sat} per Mn decreases with increasing Mn concentration. μSR results, shown in Fig. 6(d) are also consistent with the spontaneous magnetization under 10 Oe. This means $(Sr_{0.8}Na_{0.2})(Zn_{0.85}$-$Mn_{0.15})_2As_2$ is also a homogeneous ferromagnet with almost 100% ordered volume fraction at low temperatures. Fig. 6(e) shows the temperature dependence of M in H = 500 Oe for $(Sr_{1-x}Na_x)(Cd_{1-x}Mn_x)_2As_2$ with several different charge doping levels x at ZFC and FC procedures with the highest T_C 13 K.

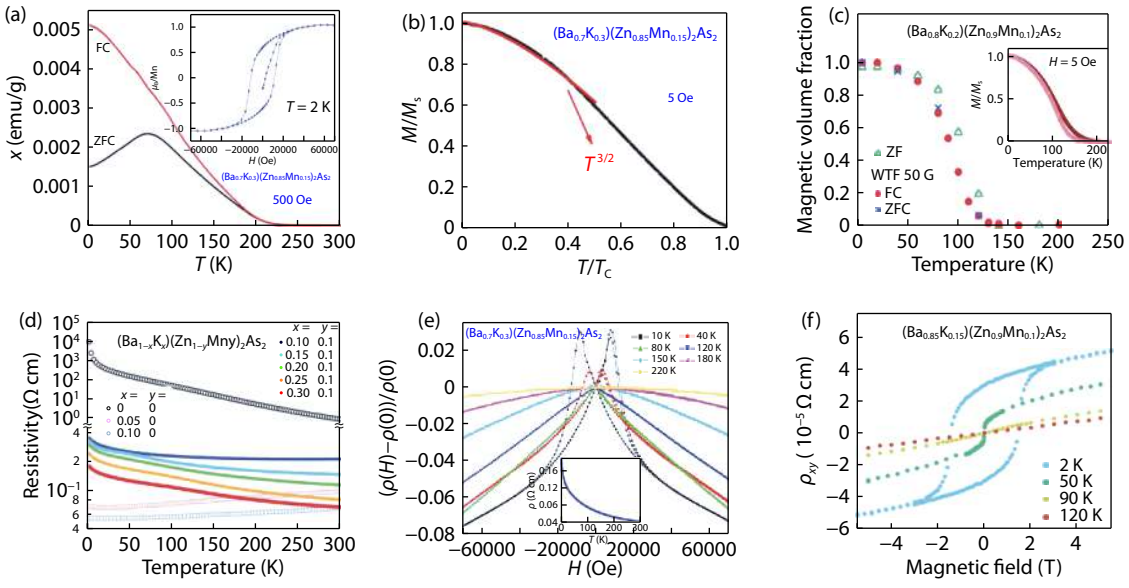

Fig. 5. (Color online) Magnetization & transport measuremets of (Ba,K)(Zn,Mn)$_2$As$_2$. (a) The tempertature dependence of M in H = 500 Oe for $(Ba_{0.7}K_{0.3})(Zn_{0.85}Mn_{0.15})_2As_2$ at ZFC and FC procedures with T_C 230 K. Inset: The isothermal magnetic hysteresis curve M(H), measured in the external field H up to 7 T. (b) The spontaneous magnetization curve under 5 Oe of $(Ba_{0.7}K_{0.3})(Zn_{0.85}Mn_{0.15})_2As_2$, showing $T^{3/2}$ dependence in low temperature expected for a homogeneous ferromagnet. (c) Volume fraction of regions with static magnetic order, estimated by μSR measurements in ZF and weak transverse field (WTF) of 50 G. No hysteresis is seen for WTF measurements with ZF cooling and field cooling in 500 G. Inset: DC magnetization results of the specimens used in μSR measurements. (d) Resistivity of $(Ba_{1-x}K_x)(Zn_{1-y}Mn_y)_2As_2$ for with several different charge doping levels. (e) Magnetoresistance curve measured in the external field up to 7 T at several selected temperatures, with obvious negative magnetoresistance below T_C. Inset: Resistivity curve of $(Ba_{0.7}K_{0.3})(Zn_{0.85}Mn_{0.15})_2As_2$. (f) Hall effect results from a sintered specimen of $(Ba_{0.85}K_{0.15})(Zn_{0.90}Mn_{0.10})_2As_2$ at several selected temperatures. A large coercive field is seen at 2 K. Adoped from Refs. [20, 22].

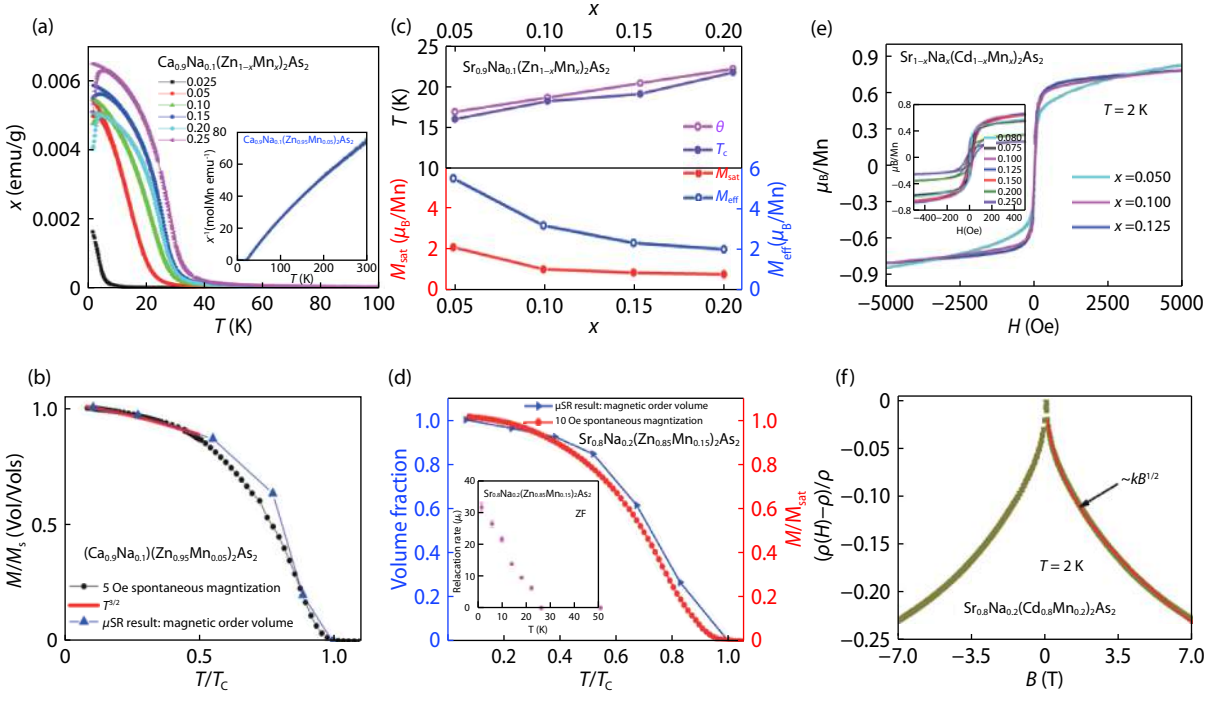

Fig. 6. (Color online) Magnetization & transport measurements of (Ca,Na)(Zn,Mn)$_2$As$_2$, (Sr,Na)(Zn,Mn)$_2$As$_2$ and (Sr,Na)(Cd,Mn)$_2$As$_2$. (a) The temperature dependence of M in H = 500 Oe for $(Ca_{0.9}Na_{0.1})(Zn,Mn)_2As_2$ with several different charge doping levels x at ZFC and FC procedures with the highest T_C 33 K. (b) The temperature dependence of the volume fraction of regions with static magnetic order, estimated by μSR measurements in ZF, consistent with that of spontaneous magnetization under 5 Oe, which shows $T^{3/2}$ dependence in low temperature expected for a homogeneous ferromagnet. (c) Curie temperature T_C, Weiss temperature θ, effective paramagnetic moment M_{eff}, and saturation moment M_{sat} for $(Sr_{0.9}Na_{0.1})(Zn_{1-x}Mn_x)_2As_2$ with different spin doping. (d) The temperature dependence of the volume fraction of regions with static magnetic order, estimated by μSR measurements in ZF, consistent with that of spontaneous magnetization under 10 Oe. Inset is the relaxation reats versus temperature, which is consistent with T_C. (e) The hysteresis curves of $(Sr_{1-x}Na_x)(Cd_{1-x}Mn_x)_2As_2$ samples with x = 0.05, 0.1, and 0.125, respectively, at 2 K. (f) Negative magnetoresistance of $(Sr_{0.8}Na_{0.2})(Cd_{0.8}Mn_{0.2})_2As_2$ at 2 K. Adoped from Refs. [40–42].

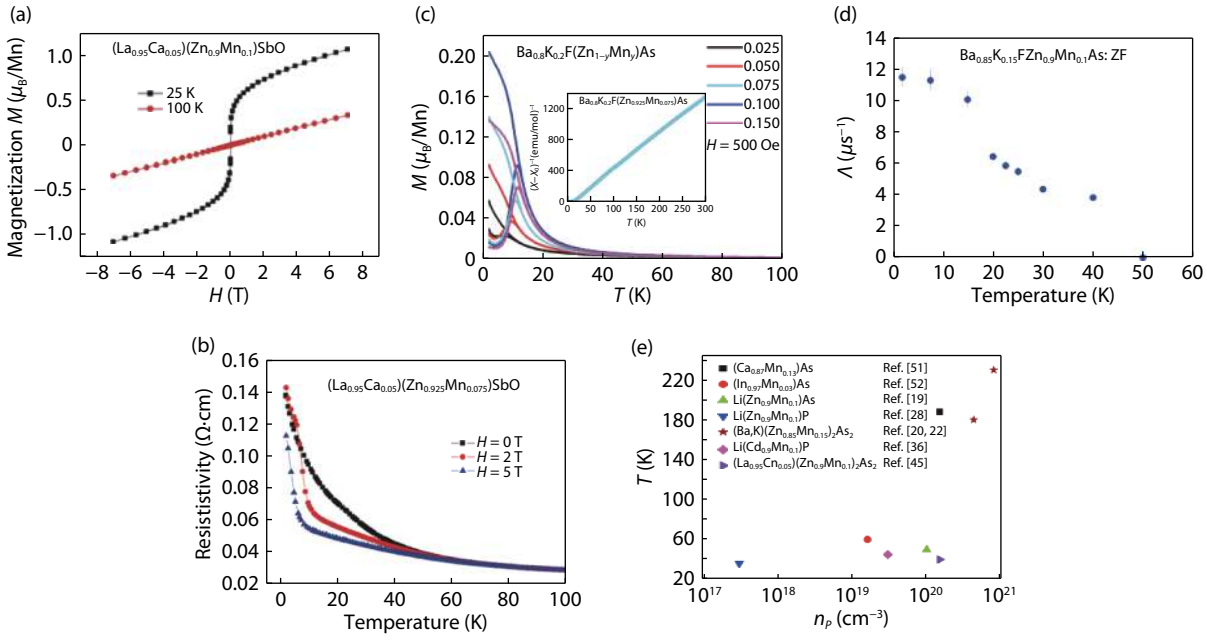

Fig. 7. (Color online) (a) Field dependences of magnetization for $(La_{0.95}Ca_{0.05})(Zn_{0.9}Mn_{0.1})SbO$ measured at 25 and 100 K. (b) resistivity of $(La_{0.95}Ca_{0.05})(Zn_{0.925}Mn_{0.075})SbO$ in various external field H, which exhibits negative magnetoresistance. (c) The temperature dependence of M in H = 500 Oe for $(Ba_{0.8}K_{0.2})F(Zn_{1-y}Mn_y)As$ with several different charge doping levels y at ZFC and FC procedures with the highest T_C 30 K. Inset shows the temperature dependence of the inverse susceptibility for $(Ba_{0.8}K_{0.2})F(Zn_{0.925}Mn_{0.075})As$. (d) The temperature dependence of fast relaxation rate Λ. The error bars represent the estimated standard deviations of the refined parameters. (e) Correlation between T_C and the hole concentration for several "111", "122", "1111" new types of diluted ferromagnetic semiconductors and typical III–V diluted ferromagnetic semiconductors. Adoped from Refs. [45, 47].

Magnetotrasport measurements performed on $(Sr_{0.8}Na_{0.2})$-$(Zn_{0.8}Mn_{0.2})_2As_2$ at 2 K under the field of up to 7 T are shown in Fig. 6(f). The negative magnetoresistance reached –23% at 2 K and 7 T Taking the orbital effect into consideration, the negative magnetoresistance data are fit by $kB^{1/2}$ rule, indicating weak localization magnetoresistance at low temperature. The similar phenomenon is found in (Ga,Mn)As system[37, 43].

2.3. "1111" type DMSs

Isostructural to the well-studied iron-based superconductor $LaFeAs(O_{1-x}F_x)$[44], a new kind of "1111" DMSs were reported after the "111" and "122" DMSs, e.g. (La,Ca)(Zn,Mn)SbO[45] and (Ba,K)F(Zn,Mn)As[46, 47], etc. Fig. 7(a) shows the *M(H)* for $(La_{0.95}Ca_{0.05})(Zn_{0.9}Mn_{0.1})SbO$ measured at 25 and 100 K, respectively. An abrupt increase of magnetization at 25 K suggests that a ferromagnetic state and paramagnetic state transition (T_C) occurs. The highest T_C reaches 40 K with proper doping in (La,Ca)(Zn,Mn)SbO material. The resistivity increases monotonically with increasing Mn concentration, suggesting that scattering center of Mn. The resistivity of $(La_{0.95}Ca_{0.05})(Zn_{0.925}Mn_{0.075})$ SbO is shown in Fig. 7(b), with magnetic field up to 5 T. A negative magnetic resistance is clearly observed in a wide temperature region. This behavior can be well explained by the field suppression of the spin fluctuation[48]. Fig. 7(c) shows the $M(T)$ in ZFC and FC procedures under 500 Oe for the $(Ba_{0.8}K_{0.2})F(Zn_{1-y}Mn_y)As$ samples with y = 0.025, 0.05, 0.075, 0.1 and 0.15, respectively. The highest T_C reaches 30 K for optimal Mn doping (y = 0.1). Above T_C, the susceptibility is fit to Curie-Weiss law as shown in the inset of Fig. 7(c), which indicates a ferromagnetic interaction between Mn^{2+}. The temperature dependence of the fast relaxation rate Λ is plotted in Fig. 7(d), exhibiting a monotonic increase with decreasing temperature and reaching a maximum value at the lowest measurement temperature (2 K). The relationships between hole concentration and T_C of "111", "122" and "1111" DMSs and other diluted ferromagnetic semiconductor systems are plotted in Fig. 7(e)[19, 20, 22, 28, 36, 45, 49, 50]. From Li(Zn,Mn)P to (Ba, K)(Zn,Mn)$_2As_2$, T_C is considerably improved. As the Zener model predicted[51, 52], the ferromagnetic ordering in DMSs is mediated by hole carriers, and the Curie temperature is positive correlated with hole concentration.

3. Properties of $(Ba,K)(Zn,Mn)_2As_2$

3.1. X ray absorption spectroscopy (XAS) & angle-resolved photoemission spectroscopy (ARPES)

The origin of magnetic ordering on DMSs is still full of debates[53–56] meanwhile the general understanding for most common (III,Mn)V–based DMSs invokes As-derived valence-band states[57, 58] as mediators of ferromagnetic interactions. As for Mn-doped II–II–V semiconductors $(Ba_{1-x}K_x)(Zn_{1-y}Mn_y)_2As_2$, the details of the electronic structure and the role of As mediating (hole) states remain unresolved both in experiment and theory. A theory[59] predicts that the competition between the short-range antiferromagnetic (superexchange) interaction and thelonger-range ferromagnetic interaction mediated by the itinerant holes determines the final ground state of BZA. Thus it is of great significance to verify the electronic states in $(Ba,K)(Zn,Mn)_2As_2$.

Fig. 8(a) exhibits the X-ray absorption spectroscopy (XAS) measurements[60] of the Mn $L_{2,3}$ edge on $(Ba_{0.7}K_{0.3})(Zn_{0.85}Mn_{0.15})_2As_2$. The line shapes of $(Ba_{0.7}K_{0.3})(Zn_{0.85}Mn_{0.15})_2As_2$ are similar to $(Ga_{0.922}Mn_{0.078})As$[61] and $(Ga_{0.958}Mn_{0.042}N)$[62], which indicates that the valence of

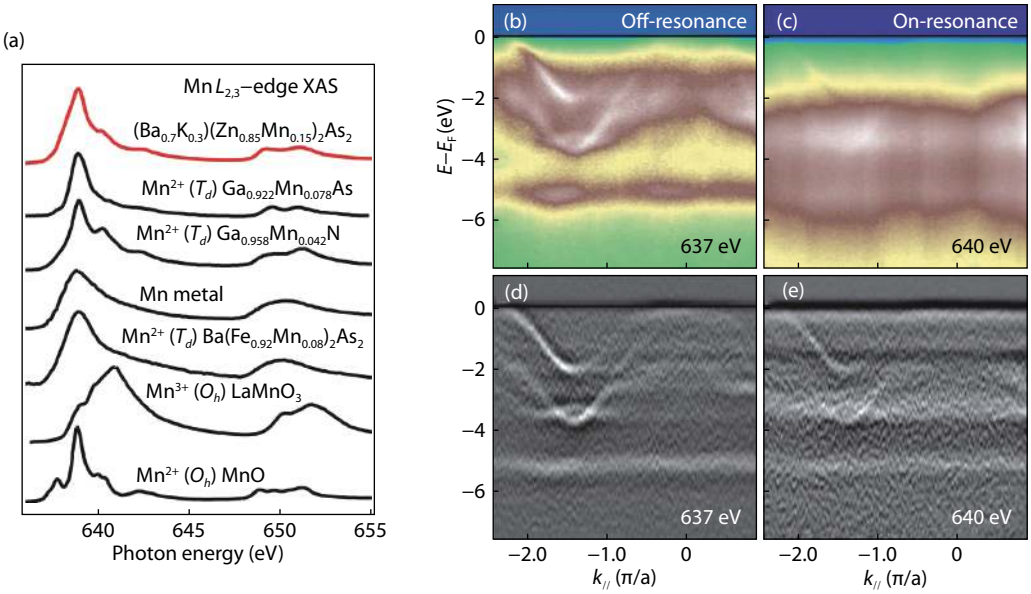

Fig. 8. (Color online) (a) Mn $L_{2,3}$-edge XAS spectra of $(Ba_{0.7}K_{0.3})(Zn_{0.85}Mn_{0.15})_2As_2$ polycrystal. The spectrum is compared with those of $(Ga_{0.922}Mn_{0.078})As$, $(Ga_{0.958}Mn_{0.042}N)$, Mn metal, $Ba(Fe_{0.92}Mn_{0.08})_2As_2$, $LaMnO_3$, and MnO.The valence and the local symmetry of the Mn atom are indicated for each compound. (b) & (c) ARPES energy-momentum intensity taken with on- and off-resonance energy photons. (d) & (e) Second derivatives of the on- and off-resonance ARPES spectra. Adoped from Refs. [60, 66].

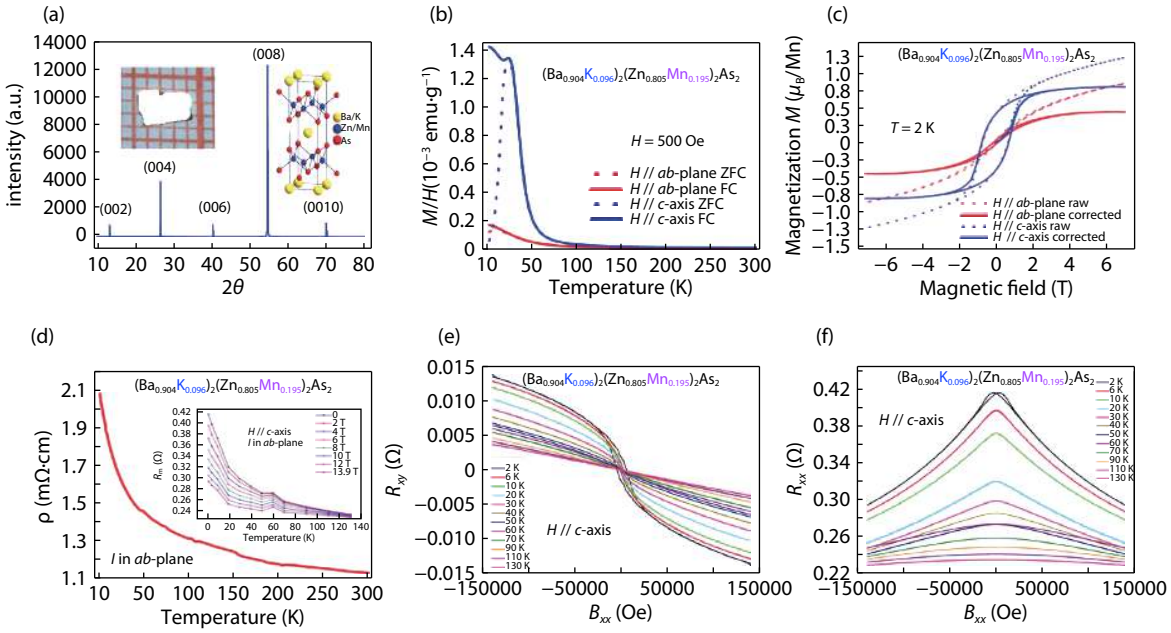

Fig. 9. (Color online) (a) The X-ray difraction patterns of $(Ba_{0.904}K_{0.096})(Zn_{0.805}Mn_{0.195})_2As_2$ at room temperature. The inset shows the crystal structure (right) and its photograph (lef). (b) The tempertature dependence of M in H = 500 Oe for at ZFC and FC procedures in c-axis and ab-plane. (c) The hysteresis curves $M(H)$ measured at 2 K in different axis to exhibit magnetic anisotropy. (d) The temperature dependence of resistivity with current in ab-plane. Inset shows the MR(T) curves in various exterial field strengths. (e) & (f) The anomalous Hall efect R_{xy} and the magnetoresistance R_{xx} at several selected temperatures from 2 to 130 K. Adoped from Ref. [67].

Mn atoms is 2+ and that Mn 3d orbitals strongly hybridize with the As 4p orbitals as in (Ga,Mn)As and (Ga,Mn)N system. The strength of hybridization is weaker than (Ga,Mn)As but stronger than (Ga,Mn)N according to the shoulder structures around $h\nu$ = 640 and 643 eV. The line shape shows a more localized nature than the Mn metal[63] and metallic Mn doped into $BaFe_2As_2$[64]. Different from $LaMnO_3$ and MnO[65], $(Ba_{0.7}K_{0.3})(Zn_{0.85}Mn_{0.15})_2As_2$ does not show the clear multiple structures, consistent with the semi-metallic conductivity in Mn-$BaZn_2As_2$[20]. Figs. 8(b)–(d) display the electronic structure of $(Ba_{0.904}K_{0.096})(Zn_{0.805}Mn_{0.195})_2As_2$ by soft X rays angle-resolved photoemission spectroscopy (ARPES)[66]. The results clarify the host valence-band electronic structure is primarily from the As 4p states. Two hole pockets around the Γ point explain the metallic behavior. The impurity band is well below the valence-band maximum (VBM), unlike that in (Ga,Mn)As, which is around the VBM. We conclude that the strong hybridization between the Mn 3d and the As 4p orbitals in $(Ba,K)(Zn,Mn)_2As_2$ plays a key role in creating the impurity band and inducing high temperature ferromagnetism.

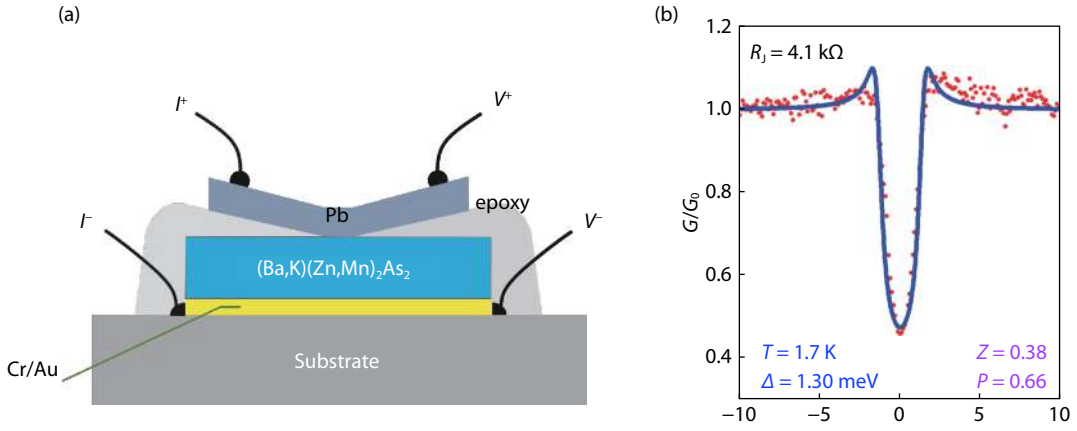

Fig. 10. (Color online) (a) Sketch of the $(Ba_{0.904}K_{0.096})(Zn_{0.805}Mn_{0.195})_2As_2$/Pb junctions used for Andreev refection spectroscopy. The inset is the normalization for the diferential conductance G/G_0. (b) Normalized diferential conductance G/G_0 spectra (red dot) and their fts to the modifed BTK theory (blue line) at selected temperatures at 1.7 K. Adoped from Ref. [67].

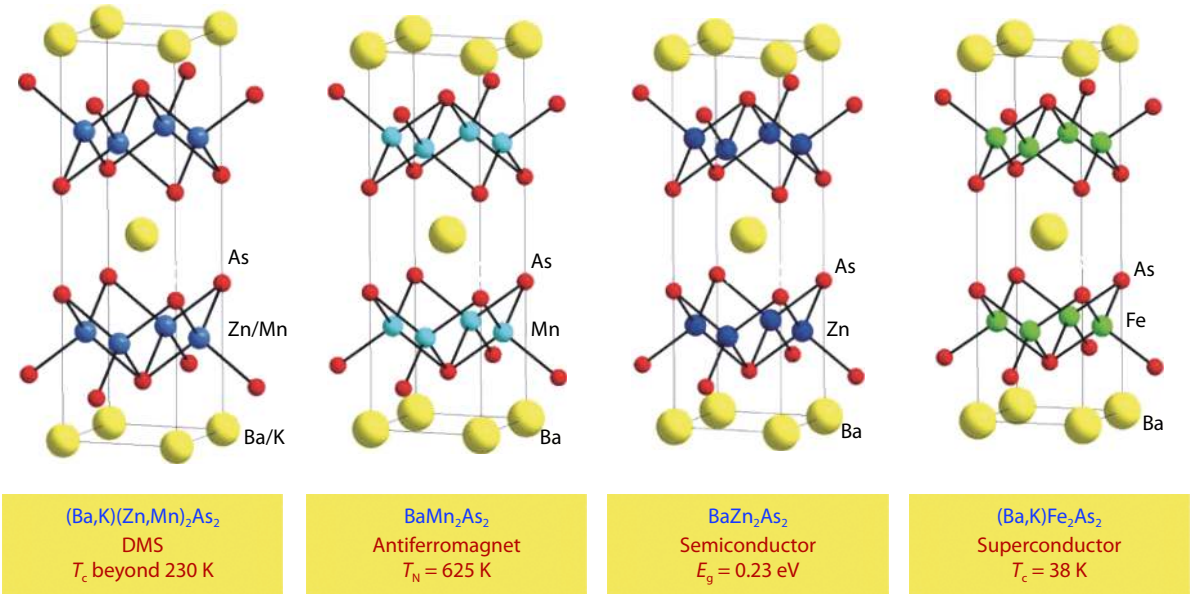

Fig. 11. (colour online) Crystal structures and key physical propertity of $(Ba,K)(Zn,Mn)_2As_2$, $BaMn_2As_2$, $BaZn_2As_2$ and $(Ba,K)Fe_2As_2$.

3.2. Single crystal growth and spin polarization measurements

Compared with polycrystals, single crystals are ideal research platforms due to fewer defects. $(Ba,K)(Zn,Mn)_2As_2$ single crystal[67, 68] is grew with flux method as shown in the inset of Fig. 9(a). Fig. 9(b) demonstrates the magnetization curves in different directions with T_C of about 50 K. Large anisotropic behavior are shown in Fig. 9(c) with easy axis along *c*. The semiconductor behavior on Fig. 9(d) arises from the localization effect[69]. Based on the Magnetoresistance R_{xx} and Hall effect R_{xy} measurements, the hole carrier density increase from 2.82×10^{20} cm^{-3} at 2 K to 4.80×10^{20} cm^{-3} at 130 K. The arise is from the enhanced thermal excitation from the impurity band to the conduction band.

Andreev refection spectroscopy (AR spectroscopy) is commonly used to achieve spin polarization (P) in various materials, e.g., (Ga,Mn)As[70], (Ga,Mn)Sb[71], $(La,Sr)MnO_3$[72], CrO_2[73], EuS[74], and $HgCr_2Se_4$[75]. A schematic view of the BZA/Pb heterojunction is shown in Fig. 10(a). A "clean" interface, represented by the parameter Z, is a crucially required in spectral analysis. For this the experiment, the small Z value ($Z = 0.38 \ll 1$) implies the manifestation of a clean and transparent interface between BZA single crystal and Pb film. One key parameter for analysis is the differential conductance, $G(V) = dI(V)/dV$. It is measured as a function of dc-bias voltage (V) crossing the AR junction. Fig. 10(b) shows normalized differential conductance G/G_0 spectra (red dot) and their best fits to the modified Blonder–Tinkham–Klapwijk (BTK)[76] theory (blue line) at 1.7 K. Spin polarization of 66% is obtained. Besides, about 40%–60% spin polarization is also achieved in a new DMSs $(Ba,Na)(Zn,Mn)_2As_2$[77]. The success on AR junction paves a solid route to fabricate multilayer heterojunctions based on BZA.

Compared to classical DMSs, new type of DMSs has one great advantage, existence of numerous isostructual function materials. As shown in Fig. 11, $(Ba,K)(Zn,Mn)_2As_2$ shares the same tetragonal $ThCr_2Si_2$ type structure with semiconductor $BaZn_2As_2$, antiferromagnetic $BaMn_2As_2$[78] and superconductor $(Ba,K)Fe_2As_2$[79]. The negligible mismatch of lattice constants in the a-b plane (less than 5%)[20] makes the above materials promising to fabricate multilayer functional heterojunctions. These heterojunctions should have near perfect inter-

Table 1. Some selected properties in new diluted magnetic semiconductors with independent spin & charge doping, superconductors and antiferromagnets.

	Diluted magnetic semiconductors (Highest Curie temperature T_C)			Superconductors (Superconducting temperature T_C')		Antiferromagnets (Neel's temperature T_N)	
Type	Structure	Material	T_C (K)	Material	T_C' (K)	Material	T_N (K)
"111"	Zinc blende type structure (F-43m)	Li(Zn,Mn)As[19]	50	LiFeAs[26] (P4/nmm)	18	LiMnAs[82] (P4/nmm)	378.3
		34					
		Li(Cd,Mn)P[36]	45				
		Li(Zn,Co,Mn)As[33]	40				
		Li(Zn,Cu,Mn)As[34]	33				
"122"	Tetragonal $ThCr_2Si_2$ type structure (P4/nmm)	(Ba,K)(Zn,Mn)$_2$As$_2$[20, 22, 60, 64, 84–88]	230	(Ba,K)Fe$_2$As$_2$[79] (P4/nmm)	38	BaMn$_2$As$_2$[78] (P4/nmm)	625
		(Ba,K)(Zn,Mn)$_2$P$_2$[89]	Theory				
		Mn-doped BaZn$_2$Sb$_2$[90]					
		(Ba,K)(Zn,Mn)$_2$(As,Pn)$_2$ (Pn = P, Sb)[83]	185				
		(Ba,Na)(Zn,Mn)$_2$As$_2$[77]	20				
		Ba(Zn$_{1-2x}$Mn$_x$Cu$_x$)$_2$As$_2$[91]	44				
		(Ba,K)(Cu,Mn)$_2$Se$_2$[92]	18				
		Ba(Zn,Co)$_2$As$_2$[80]	45				
	Hexagonal $CaAl_2Si_2$ type structure (P-3m1)	(Ca,Na)(Zn,Mn)$_2$As$_2$[40]	33				
		(Sr,Na)(Zn,Mn)$_2$As$_2$[42]	24				
		(Sr,Na)(Cd,Mn)$_2$As$_2$[41]	13				
		(Sr,K)(Zn,Mn)$_2$As$_2$[93, 94]	12				
		(Ba,K)(Cd,Mn)$_2$As$_2$[95]	16				
"1111"	ZrCuSiAs type structure (P4/nmm)	(La,Ca)(Zn,Mn)SbO[45]	40	LaFeAs(O,F)[44] (P4/nmm)	26	LaMnAsO[96] (P4/nmm)	317
		(La,Ca)(Zn,Mn)AsO[45, 97]	30				
		(La,Ba)(Zn,Mn)AsO[98, 99]	40				
		La(Zn,Mn)AsO[100]	Theory				
		(La,Sr)(Cu,Mn)SO[101]	200				
		(La,Sr)(Zn,TM)AsO[101, 102] (TM = Mn, Fe, Co)	30				
		(Ba,K)F(Zn,Mn)As[47]	30				
		La(Zn,Mn,Cu)SbO[103]	15				
		La(Zn,Mn,Cu)AsO[104]	8				
		SrF(Zn,Mn,Cu)Sb[105]	40				

face that enable deep insight of many new physical pheromones and physical rules. Recently, a series of single-phased, single-oriented thin (Ba,K)(Zn,Mn)$_2$As$_2$ films are successfully fabricated by pulsed laser deposition (PLD) on different substrates, e.g. LSAT, $SrTiO_3$, $LaAlO_3$, Si and $MgAl_2O_4$. A n-type polycrystalline BZA DMSs Ba(Zn,Co)$_2$As$_2$[80] was reported recently. All these results offers much research room for many kinds of heterojunctions in the future[4].

4. Summary and outlook

There are three main group of new diluted magnetic semiconductors with independent charge and spin doping, i.e. the "111", "122" and "1111" type, as listed in Table 1. BZA is unique in that it has T_C above 200 K. Note that there are other four DMSs which are isostructural to BZA but have low T_C. What makes BZA so special is one open question. The accurate answer to the question could be the clue to seek mechanism of DMSs and the guiding light to search for room temperature ferromagnetic DMSs.

Taking the advantage of lattice matched superconductors, semiconductors and antiferromagnetic compounds, these new types of DMSs have potential to fabricate multilayer heterojunctions[3, 4]. In the roadmap[81] for spintrionic materials, BZA is proposed as one of the most promising DMSs materials.Two major research fields are recommended for future studies of BZA: (I) to search for Curie temperature higher than room temperature based on the enhancing ferromagnetism interactions; (II) to fabricated isostructural DMSs junctions with various lattice matched materials.

Acknowledgment

We would like to thank the collaborators Prof. Y. J. Uemura, Prof. Yong Qing Li, Prof. A. Fujimori, Prof. S. Maekawa, Prof. Bo Gu, Prof. Lixin Cao, et al. We are grateful to Prof. L. Yu, F. C. Zhang, J. H. Zhao and F. L. Ning for the helpful discussions. This work is financially supported by Ministry of Science and Technology of China (Nos. 2018YFA03057001, and 2017YFB0405703), National Natural Science Foundation of China through the research projects (No. 11534016).

References

[1] Hamaguchi C. Basic semiconductor physics. Springer, 2001
[2] Mack C A. Fifty years of Moore's law. IEEE Trans Semicond Manufac, 2011, 24, 202
[3] Žutić I, Fabian J, Das Sarma S. Spintronics fundamentals and applications. Rev Mod Phys, 2004, 76, 323
[4] Žutić I, Zhou T. Tailoring magnetism in semiconductors. Sci Chin

Phys, Mechan Astronom, 2018, 61, 067031
[5] McGuire T R, Argyle B E, Shafer M W, et al. Magnetic properties of some divalent europium compounds. J Appl Phys, 1963, 34, 1345
[6] Berger S B, Pinch H L. Ferromagnetic resonance of single crystals of $CdCr_2S_4$ and $CdCr_2Se_4$. J Appl Phys, 1967, 38, 949
[7] Furdyna J K. Diluted magnetic semiconductors. J Appl Phys, 1988, 64, R29
[8] Story T, Galazka R R, Frankel R B, et al. Carrier-concentration-induced ferromagnetism in PbSnMnTe. Phys Rev Lett, 1986, 56, 777
[9] Samarth N, Furdyna J K. Diluted magnetic semiconductors. Proc IEEE, 1990, 78, 990
[10] Munekata H, Ohno H, von Molnar S,et al. Diluted magnetic III–V semiconductors. Phys Rev Lett, 1989, 63, 1849
[11] Ohno H, Shen A, Matsukura F, et al. (Ga,Mn)As: A new diluted magnetic semiconductor based on GaAs. Appl Phys Lett, 1996, 69, 363
[12] Ohno H. Making nonmagnetic semiconductors ferromagnetic. Science, 1998, 281, 951
[13] Ohno H, Munekata H, Penney T, et al. Magnetotransport properties of p-type (In,Mn)As diluted magnetic III–V semiconductors. Phys Rev Lett, 1992, 68, 2664
[14] Wang M, Campion R P, Rushforth A W, et al. Achieving high Curie temperature in (Ga,Mn)As. Appl Phys Lett, 2008, 93, 132103
[15] Chen L, Yan S, Xu P F, et al. Low-temperature magnetotransport behaviors of heavily Mn-doped (Ga,Mn)As films with high ferromagnetic transition temperature. Appl Phys Lett, 2009, 95, 182505
[16] Chen L, Yang X, Yang F, et al. Enhancing the Curie temperature of ferromagnetic semiconductor (Ga,Mn)As to 200 K via nanostructure engineering. Nano Lett, 2011, 11, 2584
[17] Dietl T. A ten-year perspective on dilute magnetic semiconductors and oxides. Nat Mater, 2010, 9, 965
[18] Bonanni A, Dietl T. A story of high-temperature ferromagnetism in semiconductors. Chem Soc Rev, 2010, 39, 528
[19] Deng Z, Jin C Q, Liu Q Q, et al. Li(Zn,Mn)As as a new generation ferromagnet based on a I–II–V semiconductor. Nat Commun, 2011, 2, 422
[20] Zhao K, Deng Z, Wang X C, et al. New diluted ferromagnetic semiconductor with Curie temperature up to 180 K and isostructural to the '122' iron-based superconductors. Nat Commun, 2013, 4, 1442
[21] Deng Z, Zhao K, Jin C. New types of diluted magnetic semiconductors with decoupled charge and spin doping. Physics, 2013, 42, 682
[22] Zhao K, Chen B, Zhao G, et al. Ferromagnetism at 230 K in $(Ba_{0.7}K_{0.3})(Zn_{0.85}Mn_{0.15})_2As_2$ diluted magnetic semiconductor. Chin Sci Bull, 2014, 59, 2524
[23] Bacewicz R, Ciszek T F. Preparation and characterization of some $A^{I}B^{II}C^{V}$ type semiconductors. Appl Phys Lett, 1988, 52, 1150
[24] Kuriyama K, Nakamura F. Electrical transport properties and crystal structure of LiZnAs. Phys Rev B, 1987, 36, 4439
[25] Kuriyama K, Kato T, Kawada K. Optical band gap of the filled tetrahedral semiconductor LiZnAs. Phys Rev B, 1994, 49, 11452
[26] Wang X C, Liu Q Q, Lv Y X, et al. The superconductivity at 18 K in LiFeAs system. Solid State Commun, 2008, 148, 538
[27] Masek J, Kudrnovsky J, Maca F, et al. Dilute moment n-type ferromagnetic semiconductor Li(Zn,Mn)As. Phys Rev Lett, 2007, 98, 067202
[28] Deng Z, Zhao K, Gu B, et al. Diluted ferromagnetic semiconductor Li(Zn,Mn)P with decoupled charge and spin doping. Phys Rev B, 2013, 88, 081203
[29] Uemura Y J, Yamazaki T, Harshman D R, et al. Muon-spin relaxation in AuFe and CuMn spin glasses. Phys Rev B, 1985, 31, 546
[30] Dunsiger S R, Carlo J P, Goko T, et al. Spatially homogeneous ferromagnetism of (Ga,Mn)As. Nat Mater, 2010, 9, 299
[31] Uemura Y J, Goko T, Gat-Malureanu I M, et al. Phase separation and suppression of critical dynamics at quantum phase transitions of MnSi and $(Sr_{1-x}Ca_x)RuO_3$. Nat Phys, 2006, 3, 29
[32] Ning F L, Man H, Gong X, et al. Suppression of T_c by overdoped Li in the diluted ferromagnetic semiconductor $Li_{1+y}(Zn_{1-x}Mn_x)P$: A μSR investigation. Phys Rev B, 2014, 90, 085123
[33] Chen B, Deng Z, Li W, et al. Li(Zn,Co,Mn)As: A bulk form diluted magnetic semiconductor with Co and Mn co-doping at Zn sites. AIP Adv, 2016, 6, 115014
[34] Guo S L, Zhao Y, Man H Y, et al. μSR investigation of a new diluted magnetic semiconductor Li(Zn,Mn,Cu)As with Mn and Cu codoping at the same Zn sites. J Phys Condens Matter, 2016, 28, 366001
[35] Sun F, Xu C, Yu S, et al. Synchrotron X-ray diffraction studies on the new generation ferromagnetic semiconductor Li(Zn,Mn)As under high pressure. Chin Phys Lett, 2017, 34, 067501
[36] Han W, Chen B J, Gu B, et al. Li(Cd,Mn)P: a new cadmium based diluted ferromagnetic semiconductor with independent spin & charge doping. Sci Rep, 2019, 9, 7490
[37] Matsukura F, Sawicki M, Dietl T, et al. Magnetotransport properties of metallic (Ga,Mn)As films with compressive and tensile strain. Physica E, 2004, 21, 1032
[38] MacDonald A H, Schiffer P, Samarth N. Ferromagnetic semiconductors: moving beyond (Ga,Mn)As. Nat Mater, 2005, 4, 195
[39] Sasaki T, Sonoda S, Yamamoto Y, et al. Magnetic and transport characteristics on high Curie temperature ferromagnet of Mn-doped GaN. J Appl Phys, 2002, 91, 7911
[40] Zhao K, Chen B J, Deng Z, et al. $(Ca,Na)(Zn,Mn)_2As_2$: A new spin and charge doping decoupled diluted ferromagnetic semiconductor. J Appl Phys, 2014, 116, 163906
[41] Chen B, Deng Z, Li W, et al. $(Sr_{1-x}Na_x)(Cd_{1-x}Mn_x)_2As_2$: A new charge and spin doping decoupled diluted magnetic semiconductors with $CaAl_2Si_2$-type structure. J Appl Phys, 2016, 120, 083902
[42] Chen B J, Zhao K, Deng Z, et al. $(Sr,Na)(Zn,Mn)_2As_2$: A diluted ferromagnetic semiconductor with the hexagonal $CaAl_2Si_2$ type structure. Phys Rev B, 2014, 90, 155202
[43] Dietl T. Interplay between carrier localization and magnetism in diluted magnetic and ferromagnetic semiconductors. J Phys Soc Jpn, 2008, 77, 031005
[44] Kamihara Y, Watanabe T, Hirano M, et al. Iron-based layered superconductor $La(O_{1-x}F_x)$ FeAs (x = 0.05–0.12) with T_C = 26 K. JACS, 2008, 130, 3296
[45] Han W, Zhao K, Wang X, et al. Diluted ferromagnetic semiconductor (LaCa)(ZnMn)SbO isostructural to "1111" type iron pnictide superconductors. Sci Chin Phys, Mechan Astronom, 2013, 56, 2026
[46] Chen B J, Deng Z, Wang X C, et al. Structural stability at high pressure, electronic, and magnetic properties of BaFZnAs: A new candidate of host material of diluted magnetic semiconductors. Chin Phys B, 2016, 25, 077503
[47] Chen B, Deng Z, Li W, et al. New fluoride-arsenide diluted magnetic semiconductor (Ba,K)F(Zn,Mn)As with independent spin and charge doping. Sci Rep, 2016, 6, 36578
[48] Bate G, Wohlfarth E. Ferromagnetic Materials. Vol. 2. Amsterdam: North-Holland Publishing Co, 1980, 381
[49] Jungwirth T, Wunderlich J, V Novák V, et al. Spin-dependent phenomena and device concepts explored in (Ga,Mn)As. Rev Mod Phys, 2014, 86, 855
[50] Ohno H, Chiba D, Matsukura F, et al. Electric-field control of ferromagnetism. Nature, 2000, 408, 944
[51] Dietl T, Ohno H, Matsukura F, et al. Zener model description of ferromagnetism in zinc-blende magnetic semiconductors. Science, 2000, 287, 1019

[52] Dietl T, Ohno H, Matsukura F. Hole-mediated ferromagnetism in tetrahedrally coordinated semiconductors. Phys Rev B, 2001, 63, 195205

[53] Jungwirth T, Sinova J, Masek J, et al. Theory of ferromagnetic (III,Mn)V semiconductors. Rev Mod Phys, 2006, 78, 809

[54] Sato K, Bergqvist L, Kudrnovský J, et al. First-principles theory of dilute magnetic semiconductors. Rev Mod Phys, 2010, 82, 1633

[55] Dietl T, Sato K, Fukushima T, et al. Spinodal nanodecomposition in semiconductors doped with transition metals. Rev Modern Phys, 2015, 87, 1311

[56] Dietl T, Ohno H. Dilute ferromagnetic semiconductors: Physics and spintronic structures. Rev Mod Phys, 2014, 86, 187

[57] Keavney D J, Wu D, Freeland J W, et al. Element resolved spin configuration in ferromagnetic manganese-doped gallium arsenide. Phys Rev Lett, 2003, 91, 187203

[58] Beschoten B, Crowell P, Malajovich I, et al. Magnetic circular dichroism studies of carrier-induced ferromagnetism in $(Ga_{1-x}Mn_x)As$. Phys Rev Lett, 1999, 83, 3073

[59] Glasbrenner J K, Žutić I, Mazin I I. Theory of Mn-doped II–II–V semiconductors. Phys Rev B, 2014, 90, 140403

[60] Suzuki H, Zhao K, Shibata G, et al. Photoemission and x-ray absorption studies of the isostructural to Fe-based superconductors diluted magnetic semiconductor$Ba_{1-x}K_x(Zn_{1-y}Mn_y)_2As_2$. Phys Rev B, 2015, 91, 140401

[61] Takeda Y, Kobayashi M, Okane T, et al. Nature of magnetic coupling between Mn ions in As-grown $Ga_{1-x}Mn_xAs$ studied by X-ray magnetic circular dichroism. Phys Rev Lett, 2008, 100, 247202

[62] Hwang J I, Kobayashi M, Song G S, et al. X-ray magnetic circular dichroism characterization of GaN/$Ga_{1-x}Mn_xN$ digital ferromagnetic heterostructure. Appl Phys Lett, 2007, 91

[63] Andrieu S, Foy E, Fischer H, et al. Effect of O contamination on magnetic properties of ultrathin Mn films grown on (001) Fe. Phys Rev B, 1998, 58, 8210

[64] Suzuki H, Yoshida T, Ideta S, et al. Absence of superconductivity in the hole-doped Fe pnictide $Ba(Fe_{1-x}Mn_x)_2As_2$: Photoemission and x-ray absorption spectroscopy studies. Phys Rev B, 2013, 88, 100501

[65] Burnus T, Hu Z, Hsieh H H, et al. Local electronic structure and magnetic properties of $LaMn_{0.5}Co_{0.5}O_3$ studied by x-ray absorption and magnetic circular dichroism spectroscopy. Phys Rev B, 2008, 77, 125124

[66] Suzuki H, Zhao G Q, Zhao K, et al. Fermi surfaces and p−d hybridization in the diluted magnetic semiconductor $Ba_{1-x}K_x(Zn_{1-y}Mn_y)_2As_2$ studied by soft x-ray angle-resolved photoemission spectroscopy. Phys Rev B, 2015, 92, 235120

[67] Zhao G Q, Lin C Q, Deng Z, et al. Single crystal growth and spin polarization measurements of diluted magnetic semiconductor $(BaK)(ZnMn)_2As_2$. Sci Rep, 2017, 7, 14473

[68] Zhao G Q, Li Z, Sun F, et al. Effects of high pressure on the ferromagnetism and in-plane electrical transport of $(Ba_{0.904}K_{0.096})$-$(Zn_{0.805}Mn_{0.195})_2As_2$ single crystal. J Phys Condens Matter, 2018, 30, 254001

[69] Nagaosa N, Sinova J, Onoda S, et al. Anomalous Hall effect. Rev Mod Phys, 2010, 82, 1539

[70] Braden J G, Parker J S, Xiong P, et al. Direct measurement of the spin polarization of the magnetic semiconductor (Ga,Mn)As. Phys Rev Lett, 2003, 91, 056602

[71] Panguluri R P, Nadgorny B, Wojtowicz T, et al. Inelastic scattering and spin polarization in dilute magnetic semiconductor (Ga,Mn)Sb. Appl Phys Lett, 2007, 91, 252502

[72] Bowen M, Bibes M, Barthélémy A, et al. Nearly total spin polarization in $La_{2/3}Sr_{1/3}MnO_3$ from tunneling experiments. Appl Phys Lett, 2003, 82, 233

[73] Coey J M D, Sanvito S. Magnetic semiconductors and half-metals. J Phys D, 2004, 37, 988

[74] Ren C, Trbovic J, KallaheR R L, et al. Measurement of the spin polarization of the magnetic semiconductorEuSwith zero-field and Zeeman-split Andreev reflection spectroscopy. Phys Rev B, 2007, 75, 205208

[75] Guan T, Lin C, Yang C, et al. Evidence for half-metallicity in n-type $HgCr_2Se_4$. Phys Rev Lett, 2015, 115, 087002

[76] Blonder G E, Tinkham M, Klapwijk T M. Transition from metallic to tunneling regimes in superconducting microconstrictions: Excess current, charge imbalance, and supercurrent conversion. Phys Rev B, 1982, 25, 4515

[77] Gu G, Zhao G, Lin C, et al. Asperomagnetic order in diluted magnetic semiconductor $(Ba,Na)(Zn,Mn)_2As_2$. Appl Phys Lett, 2018, 112, 032402

[78] Singh Y, Green M A, Huang Q, et al. Magnetic order in$BaMn_2As_2$ from neutron diffraction measurements. Phys Rev B, 2009, 80, 100403

[79] Rotter M, Tegel M, Johrendt D. Superconductivity at 38 K in the iron arsenide $(Ba_{1-x}K_x)Fe_2As_2$. Phys Rev Lett, 2008, 101, 107006

[80] Guo S, Man H, Wang K, et al. $Ba(Zn,Co)_2As_2$: A diluted ferromagnetic semiconductor with n-type carriers and isostructural to 122 iron-based superconductors. Phys Rev B, 2019, 99, 155201

[81] Hirohata A, Sukegawa H, Yanagihara H, et al. Roadmap for emerging materials for spintronic device applications. IEEE Trans Magnet, 2015, 51, 0800511

[82] Beleanu A, Kiss J, Kreiner G, et al. Large resistivity change and phase transition in the antiferromagnetic semiconductors LiMnAs and LaOMnAs. Phys Rev B, 2013, 88, 184429

[83] Peng Y, Yu S, Zhao G Q, et al. Effects of chemical pressure on diluted magnetic semiconductor $(Ba,K)(Zn,Mn)_2As_2$. Chin Phys B, 2019, 28, 057501

[84] Frandsen B A, Gong Z, Terban M W, et al. Local atomic and magnetic structure of dilute magnetic semiconductor $(Ba,K)(Zn,Mn)_2As_2$. Phys Rev B, 2016, 94, 094102

[85] Sun F, Li N N, Chen B J, et al. Pressure effect on the magnetism of the diluted magnetic semiconductor $(Ba_{1-x}K_x)(Zn_{1-y}Mn_y)_2As_2$ with independent spin and charge doping. Phys Rev B, 2016, 93, 224403

[86] Sun F, Zhao G Q, Escanhoela C A, et al. Hole doping and pressure effects on the II–II–V-based diluted magnetic semiconductor $(Ba_{1-x}K_x)(Zn_{1-y}Mn_y)_2As_2$. Phys Rev B, 2017, 95, 094412

[87] Surmach M A, Chen B J, Deng, et al. Weak doping dependence of the antiferromagnetic coupling between nearest-neighbor Mn^{2+} spins in $(Ba_{1-x}K_x)(Zn_{1-y}Mn_y)_2As_2$. Phys Rev B, 2018, 97, 104418

[88] Wang R, Huang Z X, Zhao G Q, et al. Out-of-plane easy-axis in thin films of diluted magnetic semiconductor $Ba_{1-x}K_x$-$(Zn_{1-y}Mn_y)_2As_2$. AIP Adv, 2017, 7, 045017

[89] Yang H C, Liu K, Lu Z Y. Magnetic interactions in a proposed diluted magnetic semiconductor $(Ba_{1-x}K_x)(Zn_{1-y}\ Mn_y)_2P_2$. Chin Phys B, 2018, 27, 067103

[90] Gu B, Maekawa S. Diluted magnetic semiconductors with narrow band gaps. Phys Rev B, 2016, 94, 155202

[91] Man H, Guo S, Sui Y, et al. $Ba(Zn_{(1-2x)}Mn_xCu_x)_2As_2$: A bulk form diluted ferromagnetic semiconductor with Mn and Cu codoping at Zn sites. Sci Rep, 2015, 5, 15507

[92] Guo S, Man H, Gong X, et al. $(Ba_{1-x}K_x)(Cu_{2-x}Mn_x)Se_2$: A copper-based bulk form diluted magnetic semiconductor with orthorhombic $BaCu_2S_2$-type structure. J Magnet Magnet Mater, 2016, 400, 295

[93] Yang X, Chen Q, Li Y, et al. $Sr_{0.9}K_{0.1}Zn_{1.8}Mn_{0.2}As_2$: A ferromagnetic semiconductor with colossal magnetoresistance. EPL, 2014, 107, 67007

[94] Yang J T, Luo S J, Xiong Y C. Magnetic mechanism investigations on K and Mn co-doped diluted magnetic semiconductor $(Sr,K)(Zn,Mn)_2As_2$. J Magnet Magnet Mater, 2016, 407, 334

[95] Yang X, Li Y, Zhang P, et al. K and Mn co-doped $BaCd_2As_2$: A hexagonal structured bulk diluted magnetic semiconductor

with large magnetoresistance. J Appl Phys, 2013, 114, 223905
[96] Emery N, Wildman E J, Skakle J M S, et al. Variable temperature study of the crystal and magnetic structures of the giant magnetoresistant materialsLMnAsO (L = La, Nd). Phys Rev B, 2011, 83, 144429
[97] Ding C, Guo S, Zhao Y, et al. The synthesis and characterization of 1111 type diluted ferromagnetic semiconductor ($La_{1-x}Ca_x$)-($Zn_{1-x}Mn_x$)AsO. J Phys Condens Matter, 2016, 28, 026003
[98] Jin C, Wang X, Liu Q, et al. New quantum matters: Build up versus high pressure tuning. Sci Chin Phy, Mechan Astronom, 2013, 56, 2337
[99] Ding C, Man H, Qin C, et al. ($La_{1-x}Ba_x$)($Zn_{1-x}Mn_x$)AsO: A two-dimensional 1111-type diluted magnetic semiconductor in bulk form. Phys Rev B, 2013, 88, 041102
[100] Li X, Wu X, Yang J. Control of spin in a La(Mn,Zn)AsO alloy by carrier doping. J Mater Chem C, 2013, 1, 7197
[101] Yang X, Li Y, Shen C, et al. Sr and Mn co-doped LaCuSO: A wide band gap oxide diluted magnetic semiconductor with T_C around 200 K. Appl Phys Lett, 2013, 103, 022410
[102] Lu J, Man H, Ding C, et al. The synthesis and characterization of 1111-type diluted magnetic semiconductors ($La_{1-x}Sr_x$)(Zn_{1-x}-TM_x)AsO (TM = Mn, Fe, Co). EPL, 2013, 103, 67011
[103] Zhao Y, Wang K, Guo S, et al. La($Zn_{1-2x}Mn_xCu_x$)SbO: A new diluted magnetic semiconductor isostructural to 1111-type iron pnictide superconductors. EPL, 2017, 120, 47005
[104] Guo S, Zhao Y, Gong X, et al. La($Zn_{1-2x}Mn_xCu_x$)AsO: A 1111-type diluted magnetic semiconductor with manganese and copper codoping at Zn sites. EPL, 2016, 114, 57008
[105] Fu L, Gu Y, Guo S, et al. Ferromagnetism in fluoride-antimonide SrF($Zn_{1-2x}Mn_xCu_x$)Sb with a quasi two dimensional structure. J Magnet Magnet Mater, 2019, 483, 95